Fan *et al. Chin. J. Mech. Eng.* (2018) 31:56
https://doi.org/10.1186/s10033-018-0254-1

Chinese Journal of Mechanical Engineering

ORIGINAL ARTICLE

Open Access

Plastic Deformation Mechanism in Double-Roller Clamping Spinning of Flanged Thin-Walled Cylinder

Shu-Qin Fan*, Sheng-Dun Zhao and Chao Chen

Abstract

Double-roller clamping spinning (DRCS) is a new process for forming a thin-walled cylinder with a complex surface flange. The process requires a small spinning force, and can visibly improve forming quality and production efficiency. However, the deformation mechanism of the process has not been completely understood. Therefore, both a finite element numerical simulation and experimental research on the DRCS process are carried out. The results show that both radial force and axial force dominate the forming process of DRCS. The deformation area elongates along the radial direction and bends along the axial direction under the action of the two forces. Both the outer edge and round corner of the flange show the tangential tensile stress and radial compressive stress. The middle region shows tensile tangential stress and radial stress, while the inner edge shows compressive tangential stress and radial stress. Tangential tensile strain causes a wall thickness reduction in the outer edge and middle regions of the flange. The large compressive thickness strain causes material accumulation and thus, an increase in the wall thickness of the round corner. Because of bending deformation, the round corner shows a large radial tensile strain in addition. The inner edge of the flange shows small radial compressive strain and tensile strain in thickness. Thus, the wall thickness on the inner edge of the flange continues to increase, although the increment is small. Furthermore, microstructure analysis and tensile test results show that the flanged thin-walled cylinder formed by DRCS has good mechanical properties. The results provide instructions for the application of the DRCS process.

Keywords: Flange, Double-roller clamping spinning, Plastic deformation, Cylinder

1 Introduction

Large thin-walled cylindrical parts with complex curved flanged as shown in Figure 1 are widely used in ventilator, aerospace, aeronautics and weaponry industries. Traditional processing methods use a combination of block local bending and welding, which is inefficient, and is characterized by low material utilization, poor appearance quality and poor mechanical properties. In addition, such methods cannot ensure size and geometrical tolerances.

A new double-roller clamping spinning (DRCS) process is suitable for forming large thin-walled cylindrical parts with complex curved flanges. Figure 2 shows a schematic of the DRCS process. Prior to the DRCS process, a thin-walled cylindrical workpiece is fixed on the internal expanding clamp, which expands radially under an axial compressive load to tightly clamp the cylindrical workpiece. At the same time, two rollers clamp the section, which is to be formed into a flange, and exert flanging force. The axial contact length between the rollers and workpiece is exactly the width of the forming flange. In the DRCS spinning process, the workpiece rotates together with the clamp, while the two rollers rotate on their own axis, performing three degrees of freedom motion driven by the spinning head (linear motion along the Z and X axes, and rotation around the Y axis). Thus the thin-walled cylindrical part with a complex curved flange can be formed.

The spinning process is classified as power spinning and conventional spinning, and the power spinning

*Correspondence: sunnyfan@xjtu.edu.cn
School of Mechanical Engineering, Xi'an Jiaotong University, Xi'an 710049, China

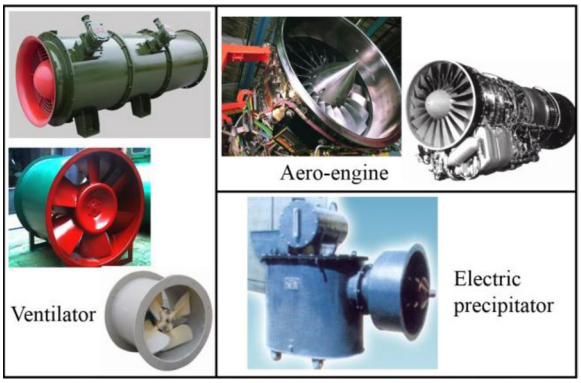

Figure 1 Typical thin-walled cylindrical part with complex curved flange

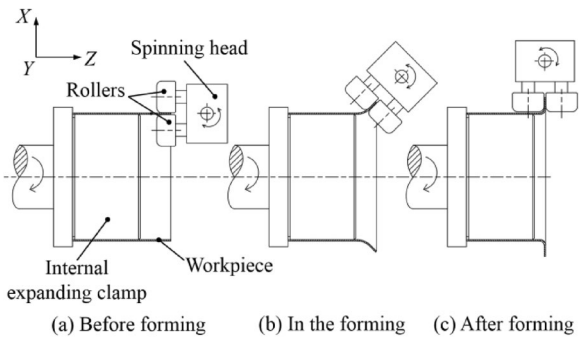

Figure 2 Schematic of the DRCS process

includes tube spinning and shear spinning [1–4]. Many researchers have investigated power spinning. Hua et al. [5] simulated a practical three-roller backward tube spinning process, particularly the bell-mouth, build-up and bulging in the spinning process, and drew the conclusion that the circumferential and axial tensile stresses cause cracks on the tube surfaces. Lexian et al. [6] developed a FE code to simulate the hot tube spinning process of the dome and obtained optimum values for the roller nose radius and release angle. Jiang et al. [7] used theoretical and experimental methods to study a ball spinning process, which belongs to tube spinning by using balls as deformation tools instead of rollers. They concluded that the radial spinning force component plays a significant role in the ball spinning of a thin-walled tube, and increasing the radial spinning force component contributes to the plastic deformation of the spun tubular blank as well as the accuracy of the spun workpieces. Mohebbi et al. [8] studied the evolution of redundant strains in a single-roller flow forming process in one pass, and concluded that frictional work can be neglected in comparison with redundant work. Parsa et al. [9] simulated the forward flow forming of tubes, calculated the flow formability of tube materials, and evaluated the effects of attack angles and feed rates on flow formability. Mori et al. [10] developed a hot shear spinning process that eliminates casting defects while forming aluminium alloy parts. Zhan et al. [11] established a three-dimensional (3D) FE model of a cone spinning process with two symmetrical rollers, and analyzed the effects of roller feed rate on spinning force and forming quality. Xia et al. [12] derived calculation formulas for the spinning forces in the flexible spinning of a cone and assessed the effects of the main process parameters using experimental and theoretical methods. Wang et al. [13] studied a stagger spinning process which is a special tube spinning process, and developed a 3D FE model of a stagger spinning process to improve the accuracy and reliability of the simulation. Zhao et al. [14] studied uneven plastic deformation in the multi-pass hot power backward spinning of high-strength cast aluminum alloy tubes to avoid defects such as cracks, bulges, and bell mouths using FE simulations and experiments. Zhan et al. [15] developed a new plastic forming technology: the rolling-spinning of titanium alloy tube, which combines rolling with tube spinning. The researchers achieved damage prediction for the rolling-spinning process. Xu et al. [16] studied the deformation characteristics and spinning forces during tube spinning with different roller distribution modes.

Moreover, significant research was carried out on conventional spinning. Kang et al. [17] reported that deformation in the first pass of conventional spinning determines the wall thicknesses of the final spun parts. Liu et al. [18] carried out research on the first pass of the spinning process using an elasto-plastic FE method. Xia et al. [19] studied the characteristics of the one-pass deep drawing spinning of cups and obtained forming limit diagrams and proper process parameters. Hamilton et al. [20] studied the material deformation mechanism of single-pass conventional spinning. Watson et al. [21] studied the material wrinkling failure mechanics of conventional metal spinning, and the effects of process parameters and material properties on wrinkling. Khaled et al. [22] proposed a new deep spinning process, using a roller set with constant clearance blank-holders to suppress wrinkle formation in the deformation zone, and also discussed the new failure modes of flange jamming and wall fractures. Roy et al. [23] constructed a novel industrial-scale apparatus and carried out spinning process experiments for a common aluminum automotive casting alloy (A356) at elevated temperatures. In addition, they established a coupled thermomechanical FE model with the various thermal and mechanical processing steps, and simulated the spinning process. Based on their experimental and simulation results, they quantified

the processing history and predicted the final geometry. Yoshihiko et al. [24] studied the effects of different pass set parameters on formability in the synchronous multi-pass spinning of a circular cup and rectangular box. Jia et al. [25] established an FE model of square section dieless spinning, obtained a relationship between surface quality and half-cone angel, and assessed the effect of the roller nose radius on surface quality.

DRCS is a type of conventional spinning process; therefore, it has many of the same advantages as conventional spinning. For example, rollers apply pressure to the local section of a workpiece, which produces local plastic deformation. Therefore, less force is needed than that in conventional pressure processing. Thus, the forming load capacity and equipment cost of DRCS is significantly reduced. In addition, DRCS can produce the products with high mechanical strength and good surface quality. It is worth mentioning that DRCS has some advantages that conventional spinning lacks.

Conventional spinning is a single-roller spinning process. Because only one roller is used, one side of the sheet metal bears severe asymmetrical spinning force, which can easily cause wrinkling. And point contact between the single roller and sheet metal causes very small plastic deformation after each spinning pass, which leads to more spinning passes and low production efficiency. Furthermore, conventional single-roller spinning requires the use of different sizes of rollers for different materials, shapes, and sizes of spun parts. These rollers have complex surface profiles, terrible stress conditions, low life cycled, and high manufacturing costs. In contrast, the new DRCS process uses two cylinder rollers with simple shapes and low costs to symmetrically clamp the sheet metal which bears compressive stress. Because there is sufficient pressure in the thickness direction, it is not easy to cause sheet wrinkling, and the spun parts have high dimensional accuracy. In contrast with conventional spinning, the DRCS process involves line contact between the rollers and sheet metal. Thus, the loading action area is larger than that in conventional spinning, and the plastic deformation in each spinning pass is larger. Consequently spinning efficiency is higher. In addition, in the DRCS process, the shape of the final parts is determined by the roller path, not by the profile of the mandrel, which is different from conventional spinning processes. That is, DRCS is a dieless, flexible spinning process that can be used to produce a variety of shapes of flanges, including rectangular flanges.

As a special type of conventional spinning process, DRCS should be studied to reveal its deformation mechanism. Thus, the authors used two methods to establish FE model of DRCS for a cylinder with a rectangular flange. The first method is the same as that for actual working conditions, where the workpiece rotates around its own axis. The second method makes the workpiece motionless, unlike in the actual forming process. Different methods may be chosen according to the different computing conditions [26]. To save computing time, the authors used the second method to establish an FE model of the DRCS, and solved key problems in establishing the model, such as the expression of the complex roller path, meshing, the clamping position for the internal expanding clamp, and the location of the bending point. Then, a precise three-dimensional elasticoplastic FE model was established for DRCS, and the FE model was verified by experiments [27]. Moreover, the authors carried out experimental research and many FE simulations and obtained the effects of main process parameters, such as the roller radius, the spacing between two rollers and the feed rate of rollers on the DRCS process [28].

Based on the above research, FE simulations and experiments on the DRCS process for rectangular flanges have been carried out in this study. DRCS spinning force, stress, strain, and wall thickness distributions for the different deformation areas have been obtained. Moreover, the mechanics performance levels of the spun parts were analyzed, and the deformation mechanism of a thin-walled cylinder with a rectangular flange was revealed.

2 FE Simulations and Experiments on DRCS Process

An ordinary Q235A steel plate was cut, rolled up, and welded to form a cylindrical workpiece. The diameter of the cylindrical workpiece was 200 mm, and its initial wall thickness was 1 mm. The diameter of the cylinder roller was 100 mm, its height was 60 mm, and its round radius was 4 mm. The main material parameters of Q235A are presented in Table 1, and its true stress–strain curve is shown in Figure 3.

Using the nonlinear FE analysis software ABAQUS/Explicit, an FE model of the DRCS process for the cylinder with the flange was established, as shown in Figure 4. Then, a DRCS simulation was carried out. Based on the G-CNC6135 general numerical control lathe, a computer-controlled experimental device for DRCS was developed to conduct the DRCS experiments. The experimental DRCS process is shown in Figure 5.

Table 1 Main material parameters

Parameter	Value
Young's modulus E (GPa)	210
Poisson ratio υ	0.3
Density ρ (kg/m^3)	7850
Yield stress σ_s (MPa)	200

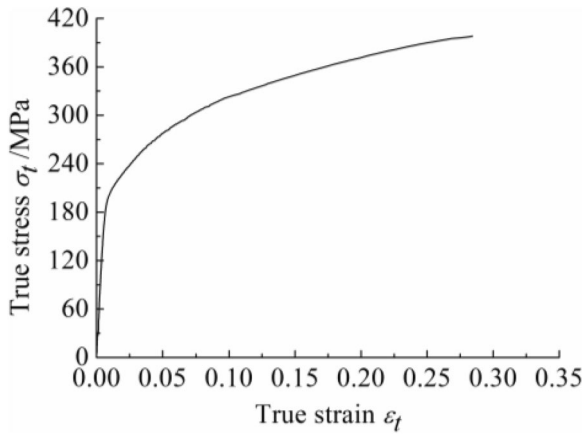

Figure 3 True stress–strain curve for material

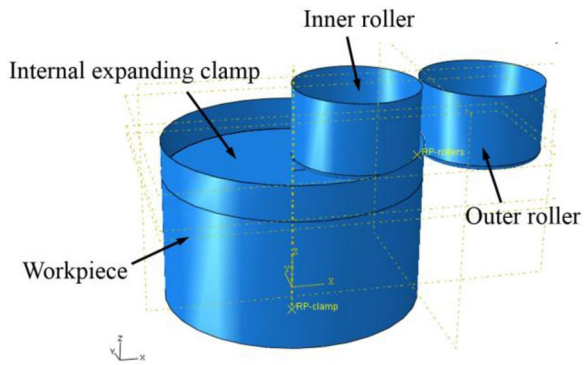

Figure 4 FE model of DRCS

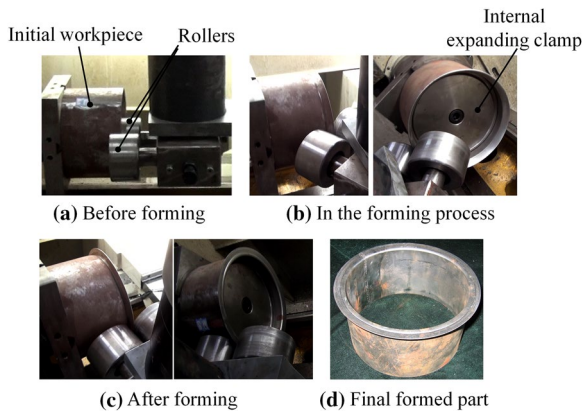

Figure 5 Experimental process of DRCS

3 Results and Discussion

Using the cylindrical workpiece with an initial wall thickness of 1 mm and diameter of 200 mm, the FE simulation has been completed. The contact length of a workpiece with rollers before spinning is referred to as the contact length *l*. The contact length is 20 mm in the simulation. In addition, the roller feed rate is defined as the rotating angle of the rollers when the workpiece rotates through a complete cycle around the main spindle. The roller feed rate is 0.05 rad/r in the simulation. Figure 6 shows variations in the equivalent strain field on the deformation zone during the forming process of DRCS.

It can be seen that throughout the process the outer edge of the deformation zone shows the largest plastic strain. The equivalent strain in the deformation zone decreases gradually along the axial direction, with the minimum value appearing on the inner edge of the deformation zone. As the forming process continues, the equivalent strain distribution does not change, but the equivalent strain in the deformation zone increases, with bending deformation becoming severe.

3.1 Spinning Force

Figure 7 shows variation curves for radial force, axial force, and tangential force. It can be seen that radial force and axial force dominate, and are greater than the tangential force throughout the DRCS process. The flange deformation area elongates along the radial direction under the action of radial force, and bends along the axial direction under the action of axial force. Before 1 s, the radial force is greater than the axial force, and radial elongation is the main deformation on the flange. At approximately 1 s, axial force is almost equal to radial force, and thus the flange is simultaneously bent by axial force and stretched by radial force. Then, after 1 s, axial force is greater than radial force, so the axial bending of the flange is more obvious than the radial elongation. The tangential force emerges because of circumferential friction, and a small friction coefficient value is chosen in the simulation, so that tangential force remains invariable during the forming process.

3.2 Stress

In the simulation, the whole DRCS process is completed within 2 s, and the stresses and strains at 1 s are chosen for analysis. For convenience, record the point at the extreme outer edge of the flange as the initial point. Choose a path composed of 32 points with different distances from the corresponding initial point, as shown in Figure 8.

The distribution in stresses on the roller contact area is different than it is on the rest of the flange, as can be seen in Figure 9. It can be seen that the roller contact area is under compressive tangential stress, and the remaining area is under tensile tangential stress. The roller contact area will show reduced compressive tangential stress

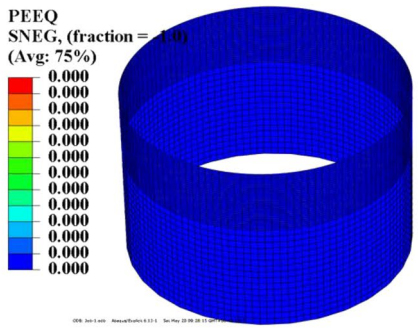

(a) Initial state

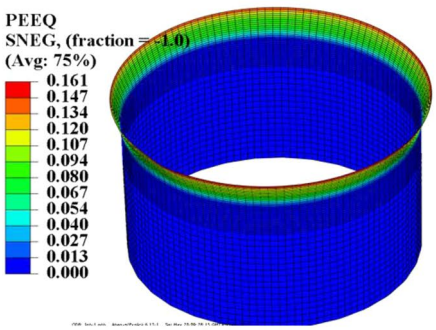

(b) 25%

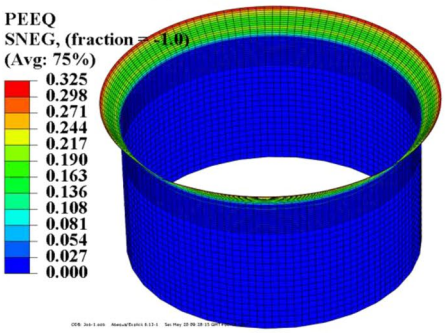

(c) 50%

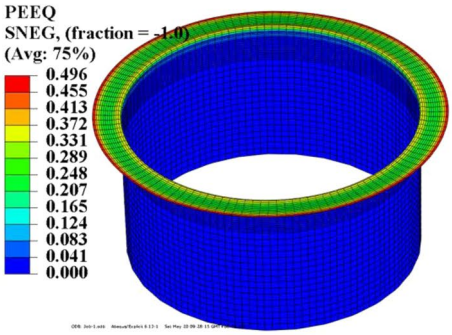

(d) 100%

Figure 6 Forming process of DRCS

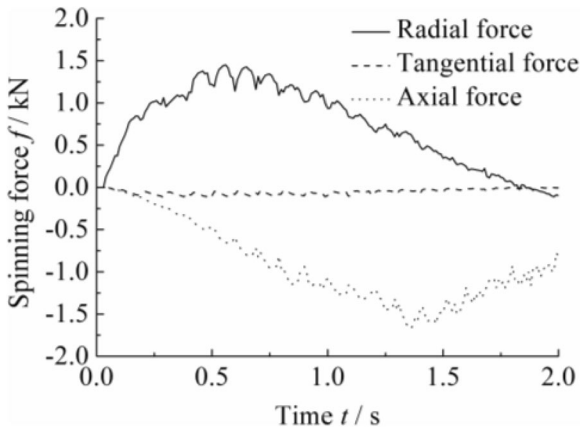

Figure 7 Variations in spinning force

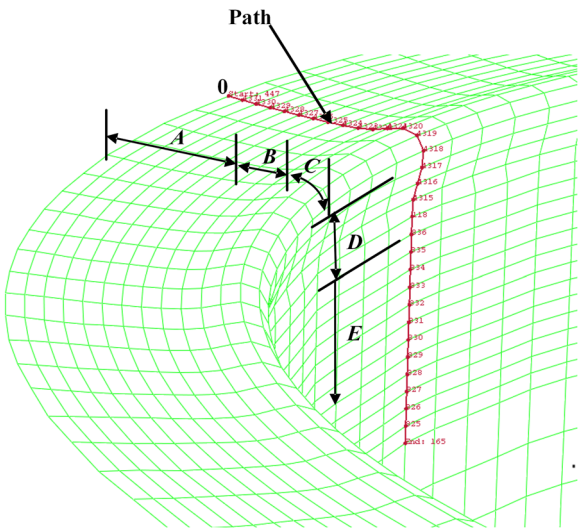

Figure 8 Path on deformation area

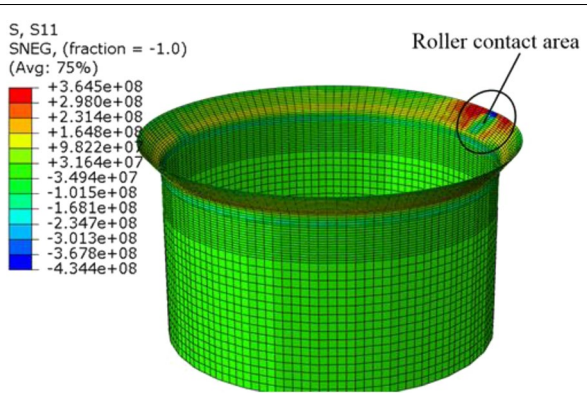

Figure 9 Distribution of tangential stress

after the roller is removed, and can even show small tensile tangential stresses.

In this study, the stress distribution on the flange after the roller is removed is focused, so the path is chosen at a location far away from the roller contact area. Adopt the distances between the points on the path and initial point as the abscissa, and take the stress values of the points on the path as the ordinate. Then the distribution curves for radial stress and tangential stress on the flange can be obtained as shown in Figure 10.

According to the different features of the deformation area, the deformation area is divided into five regions named *A*, *B*, *C*, *D* and *E*, as shown in Figure 8. Because no deformation occurs on the cylinder wall, all stresses are zero on region *E*. The outer edge of the flange (Region *A*) shows tensile tangential stress and compressive radial stress. The middle region of the flange (Region *B*) shows tensile tangential stress and radial stress, and the round corner (Region *C*) shows tensile tangential stress and compressive radial stress. The inner edge (Region *D*) shows compressive tangential stress and radial stress. It can be known that the inner edge of the flange may incur wrinkling because of the tangential compressive stress and radial compressive stress. Additionally, bulges can appear in the round corner because of the compressive radial stress.

3.3 Strain and Thickness

Continue to adopt the distances between the points on the path and initial point as the abscissa, and then take the strains of the points on the path as the ordinate. Curves for radial strain, tangential strain and thickness strain are shown in Figure 11. It can be seen that Region *A* shows tensile tangential strain, compressive radial and thickness strain, and that the absolute value of tangential strain is the largest, Thus, the wall thickness reduction in Region *A* is caused primarily by the tangential tensile strain, and the wall thickness reduction is the largest, as shown in Figure 12.

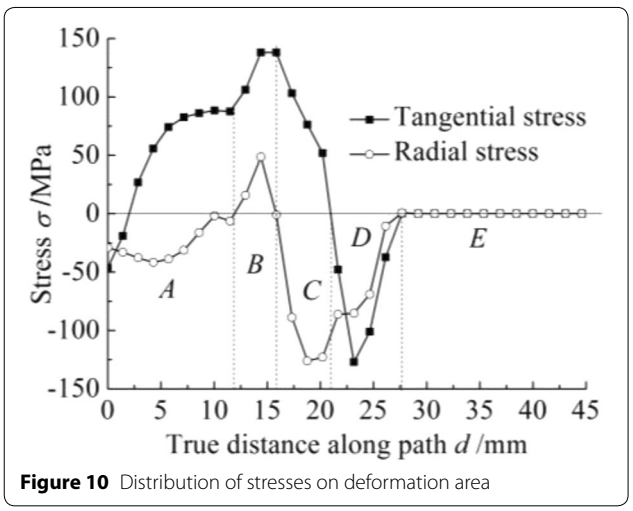

Figure 10 Distribution of stresses on deformation area

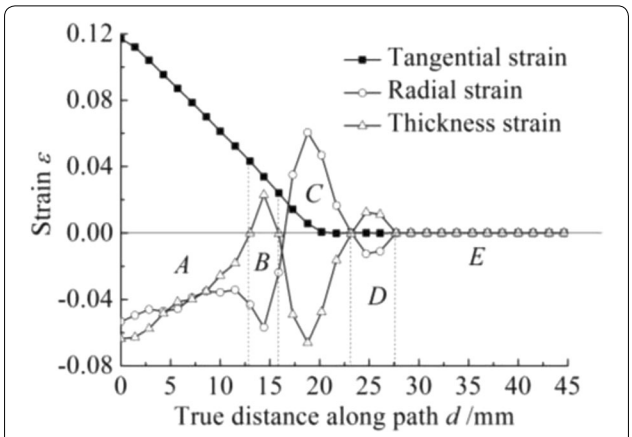

Figure 11 Distribution of strains

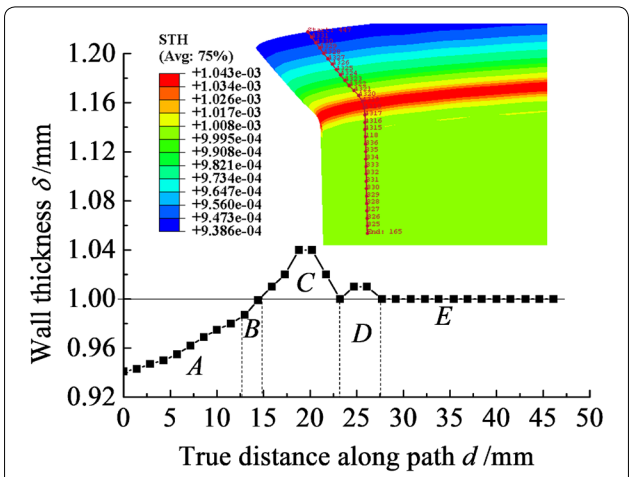

Figure 12 Distribution of wall thickness on deformation area

Region *B* shows smaller tensile tangential strain and larger compressive radial strain than Region *A*. The compressive thickness strain for Region *B* transforms into small tensile strain. The tangential tensile strain is still the main reason for the wall thickness reduction, but the wall thickness reduction decreases relative to Region *A*, which can be seen from Figures 11 and 12.

It can also be seen that the tangential tensile strain on Region *C* decreases to zero, while the thickness compressive strain increases significantly, which causes material accumulation on the round corner of the flange (Region *C*) and an the increase in wall thickness. In addition, because of bending, in Region *C* the

radial compressive strain changes to very large radial tensile strain. In Region *D*, the large radial tensile strain changes to small compressive strain, and the large thickness compressive strain changes to small tensile strain. As a result, the wall thickness on the inner edge of the flange is continues to increase, but the increment is small. No deformation occurs in Region *E*, so all strains are zero.

3.4 Microstructure Analysis

A cylinder with an initial wall thickness of 1 mm and diameter of 200 mm has been manufactured into a cylinder with a flange under the conditions of the roller contact length ($l = 20$ mm) and roller feed rate f (0.05 rad/r). Then, the formed part was cut, inlaid, ground, polished, and corroded. Both the flange area and round corner area were observed with a microscope. Figure 13(a) shows the metallographic structure of the initial blank which is mainly composed of ferrite and pearlite. Figure 13(b) and (c) show the metallographic structure of the part manufactured by DRCS. It can be seen that the material does not incur a phase change. However, the grains of the material is squashed and stretched, and they form a fibrous tissue, while the inclusions in the material are broken or stretched; therefore, the mechanical performance of the material changes. Because of the work hardening, the strength of the part increases, and its plasticity decreases.

3.5 Tensile Test for the Part Formed by DRCS

To assess changes in the strength of the part formed by DRCS, tensile tests were conducted for the parts formed by DRCS. First, a cylinder with an initial wall thickness of 1 mm and diameter of 200 mm was manufactured into a cylinder with a flange under a roller contact length of 20 mm and roller feed rate of 0.05 rad/r. Second, take the samples from the formed flange, as shown as Figure 14(a). The first type of samples, called I, were taken at a position 10 mm from the edge of the flange, while the second type of samples, called II were taken at a position 8 mm from the edge of the flange. The geometric dimensions of the samples are shown in Figure 14(b) and presented in Table 2. A photo of the samples is shown in Figure 14(c).

Finally, tensile tests were performed. The true stress–strain curve of the material formed by DRCS was obtained and compared with the true stress–strain curve

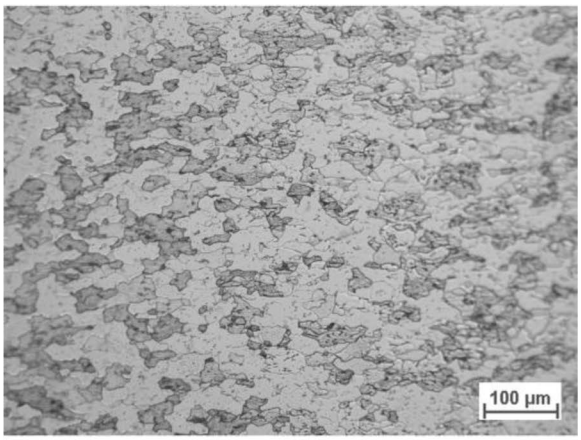

(a) Initial blank

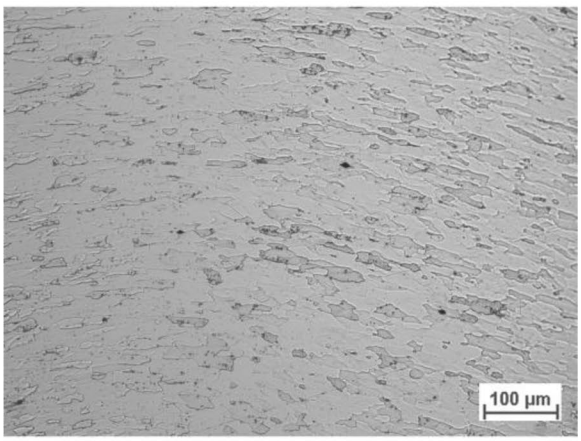

(b) Round corner area of formed part

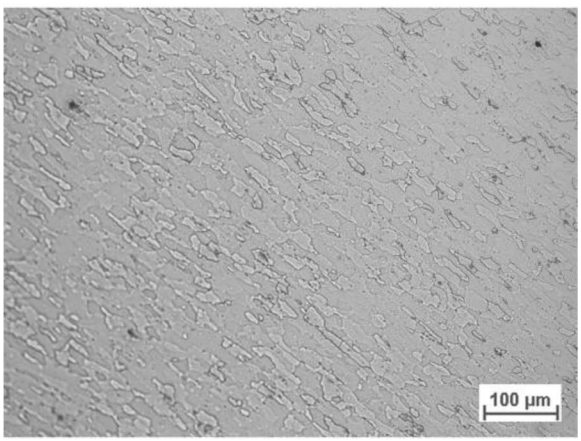

(c) Flange area of formed part

Figure 13 Metallographic structure of initial blank and part formed by DRCS (×200)

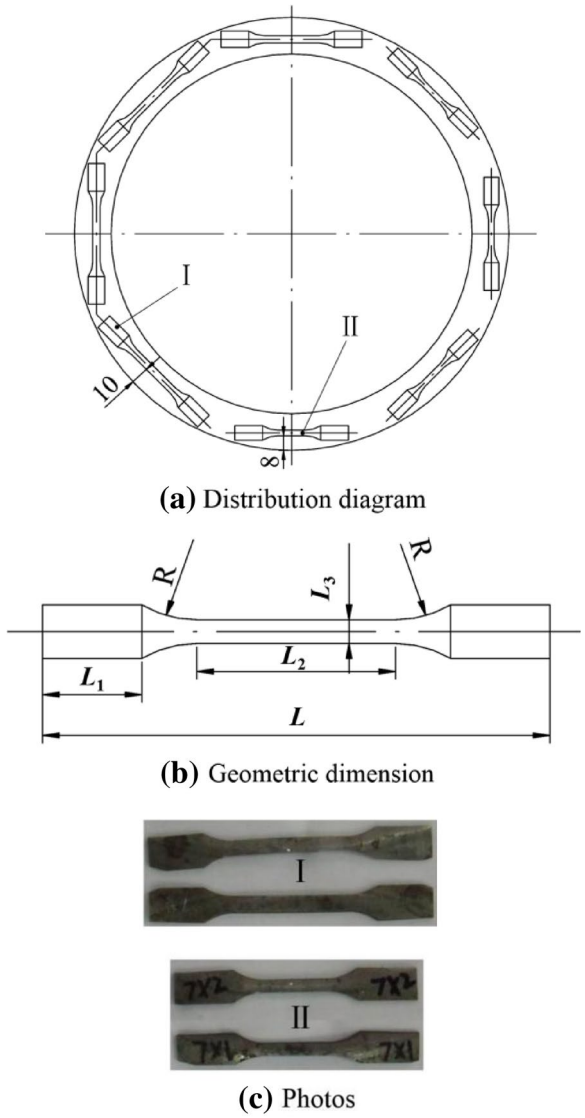

Figure 14 Samples for the tensile test

Table 2 Geometric dimension of the samples

Parameters	I	II
Overall length L (mm)	77	62
Chuck length L_1 (mm)	15	15
Original gauge length L_2 (mm)	30	15
Width L_3 (mm)	4 ± 0.03	3 ± 0.03
Knuckle radius R (mm)	15	15

of the initial material, as shown in Figure 15. The material after DRCS shows obvious work hardening, which is particularly pronounced closer to the edge of the flange.

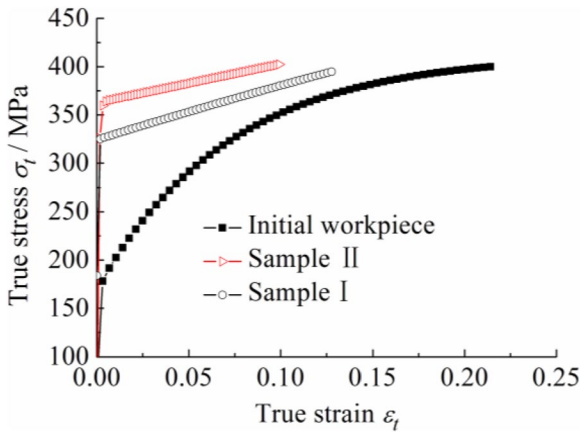

Figure 15 True stress–strain curves of the material before and after DRCS

Thus, parts formed by DRCS have high mechanical strength.

4 Conclusions

(1) Both radial force and axial force dominate the forming process of DRCS. The deformation area elongates along the radial direction under the action of radial force, and bends along the axial direction under the action of axial force.

(2) The outer edge of the flange shows tangential tensile stress and radial compressive stress, and the middle region of the flange shows tangential tensile stress and radial tensile stress. The round corner of the flange shows tangential tensile stress and radial compressive stress, and the inner edge of the flange shows tangential compressive stress and radial compressive stress.

(3) The outer edge of the flange shows tensile tangential strain, compressive radial strain, and thickness strain. The middle region of the flange shows smaller tensile tangential strain, larger compressive radial strain, and small tensile thickness strain. The tangential tensile strain causes wall thickness reduction in the two regions.

(4) The round corner of the flange shows a large thickness compressive strain, which causes material accumulation and an increase in wall thickness in this region. Because of bending deformation, the round corner also shows large radial tensile strain. The inner edge of the flange shows small radial compressive strain and the small thickness tensile strain. Consequently, the wall thickness on the

inner edge of the flange continues to increase, but the increment is small.

(5) After DRCS forming, phase changes do not happen in the material. The grains of the material get squashed and stretched, and they form fibrous tissue, and inclusions in material are broken or elongated. Thus, the strength of the workpiece increases, which indicates that the part formed by DRCS has good mechanical properties.

Authors' Contributions

CC was in charge of the whole trial; S-QF wrote the manuscript; S-DZ assisted with sampling and laboratory analyses. All authors read and approved the final manuscript.

Authors' Information

Shu-Qin Fan, born in 1977, is currently a lecturer at *School of Mechanical Engineering, Xi'an Jiaotong University, China*. She received her PhD degree from *School of Mechanical Engineering, Xi'an Jiaotong University, China*, in 2011. Her research interests include material forming theoretical analysis and numerical simulation, etc.

Sheng-Dun Zhao, born in 1962, is a professor at *School of Mechanical Engineering, Xi'an Jiaotong University, China*. He received his PhD degree from *School of Mechanical Engineering, Xi'an Jiaotong University, China*, in 1997. His research interests include plastic forming technology and equipment, computer control of mechanical–electrical-hydraulic system, fluid transmission and control, etc.

Chao Chen, born in 1990, is currently a doctoral candidate at *School of Mechanical Engineering, Xi'an Jiaotong University, China*. His research interests include advanced plastic forming technology and equipment, etc.

Competing Interests

The authors declare no competing financial interests.

Funding

Supported by National Natural Science Foundation of China (Grant No. 51305333), Shaanxi Provincial Key Science and Technology Industrial Research Plan of China (Grant No. 2014K07-23), and Shaanxi Provincial Cooperation Project of China (Grant No. 2014SJ-15).

Publisher's Note

Received: 20 September 2016 Accepted: 13 June 2018
Published online: 02 July 2018

References

[1] C H Wang, K Z Liu. *Spinning technique*. Beijing: China Machine Press, 1986. (in Chinese)

[2] Y H Zhao, Y L Li. *Spinning technology and the application*. Beijing: China Machine Press, 2008. (in Chinese)

[3] C C Wong, T A Deam, J Lin. A review of spinning, shear forming and flow forming processes. *International Journal of Machine Tools and Manufacture*, 2003, 43(14): 1419–1435.

[4] O Music, J M Allwood, K Kawau. A review of the mechanics of metal spinning. *Journal of Materials Processing Technology*, 2010, 210(1): 3–23.

[5] F A Hua, Y S Yang, Y N Zhang, et al. Three-dimensional finite element analysis of tube spinning. *Journal of Materials Processing Technology*, 2005, 168(1): 68–74.

[6] H Lexian, B M Dariani. Effect of roller nose radius and release angle on the forming quality of a hot-spinning process using a non-linear finite element shell analysis. *Proceedings of the Institution of Mechanical Engineers, Part B: Journal of Engineering Manufacture*, 2009, 223(6): 713–722.

[7] S Y Jiang, Z Y Reni. Analysis of mechanics in ball spinning of thin-walled tube. *Chinese Journal of Mechanical Engineering*, 2008, 21(1): 25–30.

[8] M S Mohebbi, A Akbarzadeh. Experimental study and FEM analysis of redundant strains in flow forming of tubes. *Journal of Materials Processing Technology*, 2010, 210(2): 389–395.

[9] M H Parsa, A M A Pazooki, M N Ahmadabadi. Flow- forming and flow formability simulation. *International Journal of Advanced Manufacturing Technology*, 2009, 42(5–6): 463–473.

[10] K Mori, M Ishiguro, Y Isomura. Hot shear spinning of cast aluminium alloy parts. *Journal of Materials Processing Technology*, 2009, 209(7): 3621–3627.

[11] M Zhan, H Yang, J H Zhang, et al. 3D FEM analysis of influence of roller feed rate on forming force and quality of cone spinning. *Journal of Materials Processing Technology*, 2007, 187–188: 486–491.

[12] Q X Xia, S Susumu. Analysis on the spinning forces in flexible spinning of cones. *Chinese Journal of Mechanical Engineering*, 2003, 16(4): 376–378.

[13] J Wang, T Ge, G D Lu, et al. A study of 3D finite element modeling method for stagger spinning of thin-walled tube. *Journal of Zhejiang University Science A: Applied Physics & Engineering*, 2016, 17(8): 646–666.

[14] G Y Zhao, C J Lu, R Y Zhang, et al. Uneven plastic deformation behavior of high-strength cast aluminum alloy tube in multi-pass hot power backward spinning. *International Journal of Advanced Manufacturing Technology*, 2016: 1–15.

[15] M Zhan, T Zhang, H Yang, et al. Establishment of a thermal damage model for Ti-6Al-2Zr-1Mo-1 V titanium alloy and its application in the tube rolling-spinning process. *International Journal of Advanced Manufacturing Technology*, 2016, 87(5): 1345–1357.

[16] W C Xu, X K Zhao, H Ma, et al. Influence of roller distribution modes on spinning force during tube spinning. *International Journal of Mechanical Sciences*, 2016, 113: 10–25.

[17] D C Kang, X C Gao, X F Meng, et al. Study on the deformation mode of conventional spinning of plates. *Journal of Materials Processing Technology*, 1999, 91(1–3): 226–230.

[18] J H Liu, H Yang, Y Q Li. A study of stress and strain distributions of first-pass conventional spinning under different roller-traces. *Journal of Materials Processing Technology*, 2002, 129(1–3): 326–329.

[19] Q X Xia, S Shima, H Kotera, et al. A study of the one-path deep drawing spinning of cups. *Journal of Materials Processing Technology*, 2005, 159(3): 397–400.

[20] Hamilton, H Long. Analysis of conventional spinning process of a cylindrical part using finite element method. *Steel Research International*, 2008, 79(1): 632–639.

[21] M Watson, H Long, B Lu. Investigation of wrinkling failure mechanics in metal spinning by Box-Behnken design of experiments using finite element method. *International Journal of Advanced Manufacturing Technology*, 2015, 78(5): 981–995.

[22] I A Khaled, S G Mohamed, G E Mohamed. Deep spinning of sheet metals. *International Journal of Machine Tools and Manufacture*, 2015, 97: 72–85.

[23] M J Roy, D M Maijer. Analysis and modelling of a rotary forming process for cast aluminium alloy A356. *Journal of Materials Processing Technology*, 2015, 226: 188–204.

[24] S Yoshihiko, A Hirohiko. Formability in synchronous multipass spinning using simple pass set. *Journal of Materials Processing Technology*, 2015, 217: 336–344.

[25] Z Jia, Z R Han, Q Xu, et al. Effects of processing parameters on the surface quality of square section die-less spinning *International Journal of Advanced Manufacturing Technology*, 2015, 80(9): 1689–1700.

[26] S Q Fan, S D Zhao, Q Zhang, et al. Finite element model determination of double rollers clamping expanding spinning for right-angle flange. *Journal of Xi'an Jiaotong University*, 2010, 44(5): 66–70. (in Chinese)

[27] S Q Fan, S D Zhao, Q Zhang, et al. Finite-element modeling of a novel flanging process on a cylinder with a large diameter-thickness ratio. *Proceedings of the Institution of Mechanical Engineers, Part B: Journal of Engineering Manufacture*, 2011, 225(7): 1117–1127.

[28] S Q Fan, S D Zhao, Q Zhang. Research on effects of roller parameters on double rollers clamping spinning. *Journal of Mechanical Engineering*, 2012, 48(18): 60–66. (in Chinese)